TITLE

Longitudinally modeling anti-neoantigen immunity under paradigms of immunodominance

AUTHORS

Timothy Qi[1], Benjamin Vincent[2,3], and Yanguang Cao[1,2*]

AFFILIATIONS

[1]Division of Pharmacotherapy and Experimental Therapeutics, Eshelman School of Pharmacy, The University of North Carolina at Chapel Hill, Chapel Hill, NC 27599, USA

[2]Lineberger Comprehensive Cancer Center, The University of North Carolina at Chapel Hill, Chapel Hill, NC 27599, USA

[3]Division of Hematology/Oncology, School of Medicine, The University of North Carolina at Chapel Hill, Chapel Hill, NC 27599, USA

*__Lead Contact__. Email: yanguang@unc.edu. Address: 301 Pharmacy Ln, Chapel Hill, NC 27599

WORD COUNT: 2,974

ABSTRACT

Neoantigen clonal architecture influences the efficacy of immunotherapy. The longitudinal dynamics of clonal neoantigen immunodominance over a canvas of heterogeneous subclonal neoantigens is critical to response durability, but challenging to characterize clinically and experimentally. We developed a computational model of neoantigen evolution that longitudinally tracks the “presentome” – that is, a cell’s aggregate neoantigen repertoire and HLA status – of simulated non-small cell lung cancer (NSCLC) prior to and during treatment with checkpoint blockade. Using well-established neoantigen immunogenicity parameters, we first recapitulated the clinically observed presentomes of early-stage NSCLC tumors. After validating simulated neoantigen burden in an independent cohort, we simulated response to PD-1 blockade in silico. In addition to recapitulating known phenomena, such as the correlation of pre-treatment clonal neoantigen burden with response to PD-1 blockade, we found several additional salient features of response, including a profound clonal collapse among completely responding tumors and an insensitivity of response to increased oligoclonality of anti-neoantigen-presenting cell cytotoxicity. Our work can be adapted to longitudinally model the neoantigen architecture of other cancers, modalities of immunotherapy, and preclinical tumor models, ultimately informing cognizant strategies for future therapeutic development.

INTRODUCTION

It remains difficult to predict immune checkpoint inhibition (ICI) outcomes a priori[1]. Neoantigens – that is, de novo tumor-specific antigens that arise from somatic genome alterations or tumor-specific RNA expression and provoke a response from the adaptive immune system – have emerged as promising prognosticators of ICI response, especially when clonally expressed[2, 3]. Tumors enriched in clonal neoantigens are more highly infiltrated by CD8+ tumor-infiltrating lymphocytes (TILs), including cognate TCR clonotypes. This often correlates with more favorable overall survival (OS) outcomes[2, 4]. Further supporting the broad importance of “immune target” clonality, a pan-cancer analysis found clonal tumor mutation burden (TMB) to correlate more closely with ICI response compared with subclonal TMB or TMB alone[5].

Conversely, subclonally expressed (neo-)antigens may be protected from immunoreactivity, as demonstrated by Gejman et al. in a series of elegant murine experiments[6]. In humans, studies of non-small cell lung cancer (NSCLC) have found that among hundreds of candidates, very few neoantigens can be validated as immunogenic ex vivo; that those that are, tend to be clonal[2, 7, 8]. These studies indicate that subclonal neoantigens below a threshold clonal fraction might be protected from immunological pruning, even if more intrinsically immunogenic than a clonally expressed neoantigen. We postulate immunodominance as a potential mechanism for this protection, whereby some antigens detract from adaptive immune responses against other antigens through their relative abundance and immunogenicity-mediated immunodominance[9].

In this work, we investigate neoantigen clonal architecture and potential immunodominance by computationally modeling tumor growth pre- and post-ICI-induced anti-tumor immunity. We refer to the most highly clonal neoantigens that preclude robust responses to subclonal neoantigens as “tumor dominant antigens”, or TDAs. Explicitly, we consider TDAs to be immunodominant (neo-)antigens with the highest intratumoral cellularity and, in situations

where multiple (neo-)antigens are equally clonal, the strongest intrinsic immunogenicity[6, 9, 10]. We show that our model can recapitulate the neoantigen architecture of untreated NSCLC[2, 11–13] and use the derived parameters to simulate a cohort of 1,051 late-stage NSCLCs under ICI. We then evaluate differences in neoantigen clonal architecture among responders and interrogate the roles of immunodominance and neoantigen architecture in influencing ICI outcomes.

METHODS

Simulated neoantigens

Tumor simulations were performed in MATLAB R2020b. Founder cells were assigned j neoantigens with immunogenicity scores r. The number of neoantigens j was drawn from a gamma distribution fit to NSCLC neoantigen burdens reported by Rosenthal et al.[12]. Generated neoantigens were first assigned random values for MHC binding affinity, MHC binding stability, agretopicity, transcript abundance, and foreignness drawn from distributions defined by 146 NSCLC-derived peptides[8]. To achieve this, we fit an exponential distribution was to transcript abundance and a zero- and one-inflated binomial distribution to foreignness. To account for correlation among MHC binding affinity, MHC binding stability, and agretopicity values, we fit a Gaussian copula.

Newly gained neoantigens were assigned values sampled from these distributions. We discarded transcript abundance due to conflation with clonality and used the remaining four features to classify the immunogenicity of generated neoantigens ("Wells' criteria"): MHC binding affinity < 34 nM, MHC binding stability > 1.4 hours, agretopicity > 0.1, and foreignness (pathogen homology) < 10^{-16}[8]. Neoantigens that failed to satisfy these criteria were assigned an immunogenicity score of 0. Neoantigens that met all criteria for likely immunogenicity were assigned an immunogenicity score r from an exponential distribution of the exponent 6 evaluated at a random point on the interval [0,1]; otherwise, they were assigned score of 0.

Cells that gained neoantigens during growth were evaluated under a similar process with j = j + 1; that is, one new neoantigen evaluated against Wells' criteria.

Simulated founder cells and tumor growth

Simulated tumors grew according to a modified logistic growth model, where N is the number of cells in the tumor, b is the deathless birth rate, k is the population carrying capacity and d is the integrated death rate.

$$\frac{dN}{dt} = N\left(b\left(1 - \frac{N}{k}\right) - d\right)$$

Founder cells were assigned a deathless birth rate b by sampling from a log normal distribution (Table S1). Each clone in a tumor was assigned the same birth rate b but a potentially different integrated death rate d, depending on immunogenicity, antigen presentation, and clonal fraction as described herein. Thus, each clone grew at different rates toward a tumor-wide carrying capacity k at a rate depending on death rate d.

Founder cells were assigned a clone ID i. Each clone was assigned three HLA alleles h, an array r containing j neoantigens, an array p of presentation mapping flags, and an array e of expression status flags. In all cases, h was assigned an initial value of {1, 1, 1}, indicating the intact status of all HLA alleles. Each tumor's founder cell had a 14% chance of losing one HLA allele prior to growth (e.g., {1, 0 1}), representing a truncal HLA loss of heterozygosity[11]. Neoantigen array r of length j stored immunogenicity scores of all neoantigens in the clone, whereas array p mapped each neoantigen to one of three HLA alleles. Finally, array e stored j values of either 0 or 1, a simplified representation indicating whether the neoantigen was productively expressed in the presentome or not due to loss in the genome, epigenome, or transcriptome. Thus, each neoantigen's presentome-level immunogenicity a could be described as

$$a_{in} = h_i(p_{in}) * r_{in} * e_{in}$$

Where n represents the neoantigen in question. Thus, all neoantigens with a > 0 were considered productively presented in the presentome and had r > 0, n = 1, and h(p) = 1.

To implement neoantigen immunodominance, clonalities for each neoantigen were calculated based on their cellularity (i.e., the fraction of cells whose presentomes productively presented it). This returned a TDA array of two neoantigens that had the highest clonality and, in the case of ties, the greatest immunogenicity scores. Clones were then assigned an immunogenicity A in the range [0,1] based on their productive presentation of a TDA:

$$A_i = \max(a_{in} \in TDA)$$

A clone's immunogenicity A was then used to determine d, its integrated death rate:

$$d_i = \begin{cases} d_0 * \left(1 + \frac{A_i}{\frac{b}{d_0}}\right) * (1 + T) & if A_i \in TDA \\ d_0 & otherwise \end{cases}$$

Where base death rate d_0 is equal to 90% of the birth rate b and T represents treatment strength (Table S1)[14]. With no treatment, death is maximally amplified by immunogenicity A = 1, under which d_i = b and the clone ceases to grow. With treatment, d_i can be further amplified to exceed b, leading to clonal shrinkage. Altogether, each individual clone's growth can be described as:

$$\frac{dN_i}{dt} = N_i \left(b_i \left(1 - \frac{\sum_{\emptyset=1}^{i} N_\emptyset}{k} \right) - d_i \right)$$

Total tumor growth was thus equal to the cumulative net growth of all clones, each of which was driven by a modified logistic growth function and shared a carrying capacity.

Pertaining to Figure 1, 100 tumors were allowed to grow to target diameters of either 1.5 cm (stage IA), 3.5 cm (stage IB), 4.5 cm (stage IIA), or 5 cm (stage IIB/III). Diameters were calculated assuming tumor sphericity and a volume of ~4.19 pL per cell (Table S1). Tumors whose diameters shrunk below 2 mm during treatment were assumed below the limit of quantification and designated CR[15].

Presentome modification by neoantigen gain, neoantigen loss, and HLA loss

Prior to growth, founder cells were assigned a neoantigen gain rate g from a log normal distribution (Table S1). Neoantigen loss and HLA loss rates were then fixed to 67% of the neoantigen gain rate (Table S1)[11, 12]. These rates were held constant across all clones within a tumor. At each timestep, tumors accumulated neoantigen gain, neoantigen loss, and HLA allele loss events at a fixed rate (Table S1). These events were randomly distributed across

living clones, such that one cell was removed from each clone assigned an event, modified according to the type of the event, and established as a distinct clone of N = 1.

Total neoantigen, presentome neoantigen, and tumor diameter estimations in the validation cohort

Neoantigen predictions reported by Forde et al. 2018 in 12 patients with sufficient pretreatment tissue to characterize candidate neoantigens were assessed. Total neoantigens were calculated by filtering positive netCTL classification. To apply Wells' criteria, we calculated agretopicity by taking the ratio of somatic and wild-type MHC binding affinity. For predictions containing somatic peptides of identical sequences but different HLA alleles, the more strongly binding prediction was used. Binding stabilities were calculated with NetMHCStabPan using default parameters[16]. The number of neoantigens that passed three of five Wells criteria (MHC binding affinity < 34 nM, MHC binding stability > 1.4 hours, and agretopicity > 0.1) was multiplied, in the absence of reported foreignness, by a correction factor equal to ratio of neoantigens in the Rosenthal et al. cohort passing the MHC binding affinity, stability, and agretopicity criteria that also did or did not adhere to the foreignness threshold of < 10^{-16}[12]. This reduced the number of predicted presentome antigens by 80.6%. As biopsies were single-region, neoantigen clonality was not assessed. Tumor diameters were estimated for each tumor using conventional NSCLC staging criteria[17]. For each of seven discrete tumor diameters, a cohort of 100 tumors was simulated.

Simulated ICI treatment

1,051 tumors were allowed to grow to target diameters of > 5 cm to represent late-stage NSCLC. Treatment was then initiated by increasing treatment strength T from 0 to 8% (Table S1), effectively increasing the death rates of only the cells with a TDA in their presentome. TDAs were not allowed to vary over the course of treatment, except during select sensitivity

analyses. Every 9 weeks on treatment, tumor diameters were assessed for classification per RECIST v1.1. To approximate the duration of four trials of anti-PD-1 monotherapy for advanced NSCLC, simulations were stopped after 54 weeks of treatment or upon CR[18–21].

Statistical analyses

Statistics were performed in MATLAB R2020b. In general, categorical distributions were assessed for statistical significance at $\alpha = 0.05$ via chi-square test. Continuous outcomes were assessed for statistical significance at $\alpha = 0.05$ using one-way ANOVA and/or post-hoc paired or unpaired Student's t-tests as appropriate. In cases of post-hoc multiple hypothesis testing, a Bonferroni correction was applied. Details of specific statistical analyses are provided in their corresponding figure captions.

RESULTS

Simulations recapitulate early-stage NSCLC neoantigen architecture

We simulated the growth of 100 NSCLC tumors and characterized their neoantigen clonal architectures using parameters derived from previous literature (Figure 1A, Table S1). To model the oligoclonality of anti-tumor adaptive immunity, the two most clonally expressed and immunogenic neoantigens at any given time were deemed TDAs, such that only cells harboring TDAs were at greater propensity to be eliminated[2, 22].

We allowed simulated tumors to grow until pre-determined sizes to approximate the TRACERx 100 cohort of 26 stage I, 36 stage IB, 13 stage IIA, and 25 stage IIB/IIIA/IIIB tumors (Figure 1C)[23]. As they grew, clones within a tumor were allowed to modify their presentomes by acquiring new neoantigens, losing extant neoantigens, and losing HLA alleles[22]. Loss of an HLA allele reduced the immunogenicity of all neoantigens presented by that allele to 0. Of note, formerly clonal neoantigens were classified as subclonal if new clones deficient in their presentation, whether through HLA or direct loss, emerged during treatment.

Simulated tumors displayed a high level of variance in their heterogeneity, with some tumors harboring solely clonal neoantigens and others harboring predominantly subclonal neoantigens (Figure 1D). Total neoantigen burdens and (sub-)clonal HLA loss fractions in our simulated cohort were similar to those reported by Rosenthal et al., 2019 and McGranahan et al., 2017, respectively (Figure 1D-E). Overall, our model could recapitulate previously reported peptide features, neoantigen clonalities, and HLA landscapes of NSCLC tumors.

Simulations recapitulate neoantigen burdens of a validation cohort

We used neoantigen burden and characteristics reported by Forde et al. to assess model generalizability to other cohorts of NSCLC patients[13]. In this study, investigators took single-region biopsies prior to administering 2 doses of anti-PD-1 over 4 weeks in the neoadjuvant setting. In total, 12 tumors had sufficient biopsy material to characterize

pretreatment neoantigen burden. We approximated tumor sizes for each and simulated a cohort of 100 tumors for each discrete size (Figure 2A). 11 of 12 total neoantigen burdens and 12 of 12 calculated presentome neoantigen burdens were within the simulated ranges of equivalently-sized simulated tumors (Figure 2B-C). In general, despite high variability, larger tumors harbored greater total and presentome neoantigen burdens.

Neoantigen burden correlates with ICI response

To simulate ICI treatment, we established a cohort of 1,051 late-stage tumors and selectively amplified the death rates of clones harboring a TDA at treatment initiation. We observed 1% complete response (CR), 29% partial response (PR), 48% stable disease (SD), and 22% progressive disease (PD) at 54 weeks per RECIST v1.1 (Figure 3B-D)[24]. These outcomes were consistent with pooled results from 4 anti-PD-1 monotherapy arms in trials of previously untreated late-stage NSCLC[19–22].

Several pre-treatment features correlated with treatment response. Pre-treatment TDA immunogenicity scores correlated strongly with response (Figure 3E). Responses were poorer in tumors with significant loss of TDA expression prior to treatment, but comparable among tumors regardless of HLA allele intactness prior to treatment (Figure 3F-G). We also found that pre-treatment total, clonal, subclonal, and clonal reactive neoantigen burden (the number of unique clonal neoantigens satisfying Wells' criteria and most likely to be functionally validated ex vivo) all correlated with treatment response (Figure 3H). In contrast, tumors that progressed under ICI tended to have greater post-treatment total and subclonal neoantigen burden and lesser post-treatment clonal (reactive) neoantigen burden, perhaps reflecting presentome diversification accompanying further tumor growth. These findings align with previous reports that tumors refractory to ICI undergo remodeling of their neoantigen architecture through loss of previously clonal antigens[4].

Neoantigen consolidation correlates with complete response

We next evaluated differences in pre- and post-treatment neoantigen burden in tumors that experienced CR under treatment versus all other tumors, which we termed “non-CR” (Figure 3I-J). Unexpectedly, CR tumors had significantly greater total and subclonal neoantigen burdens but similar clonal (reactive) neoantigen burdens as non-CR tumors prior to treatment. This relationship changed after ICI, as residual (below limit of quantification) post-treatment CR tumors had lower total and subclonal neoantigen burden but greater clonal (reactive) neoantigen burden than non-CR tumors. In parallel, simulated treatment caused a decrease in total and subclonal neoantigen burden in CR tumors compared to before treatment, but did not in non-CR tumors, similar to clinical reports of ICI-mediated neoantigen pruning[4]. There were no significant differences in sampled birth and neoantigen gain rates between CR and non-CR tumors. Intriguingly, 72% of pre-treatment tumors harbored at least one subclonal neoantigen with higher immunogenicity than their TDA (Figure 4A). After treatment, the fraction of tumors with these neoantigens, termed “subdominant TDA candidates”, grew to 88%. Together, these data suggest that while tumoral neoantigen burden can diversify after ICI, tumors that undergo CR might instead experience a consolidation of neoantigen diversity.

Simulated responses are insensitive to increased oligoclonality

We performed a sensitivity analysis by varying parameter values for TDA number, birth rate, neoantigen gain/loss rate, HLA loss rate, and treatment strength 50% (Figure 4B). Simulated treatment outcomes were insensitive to TDA number (response oligoclonality) but were sensitive to all other parameters, especially treatment strength. We also investigated the effect of our modeled TDA assumptions on outcomes. Both increasing the set of TDAs to include all neoantigens (effectively a perfectly polyclonal response with zero TDAs) as well as allowing the TDA to be recalculated each day after treatment initiation (a “rapidly-evolving” anti-tumor response) modestly affected outcomes. Overall, we saw a lack of improvement in

outcomes under increased oligoclonality and a modestly greater proportion of partial responders under polyclonality, which suggests that therapeutic strategies aiming to increase the diversity of anti-tumor T cell responses could be restricted by aspects other than TCR recognition of cognate antigen.

DISCUSSION

We developed a tumor growth model of NSCLC and used it to investigate the effects of immunodominance and neoantigen architecture on ICI outcomes. While several noteworthy computational models of neoantigen evolution have been published[25–27], these models consider either a fixed cancer cell population size[27] or calculate immunogenicity as the cumulative immunogenicity of neoantigens expressed by a lineage or clone[25, 26]. No work, to our knowledge, has modeled a growing tumor with neoantigen architecture tracking and tumor-level oligoclonal immunodominance. Our results support the directive that neoantigen discovery methods should focus not only upon neoantigen burden – a proxy for diversity – but also upon neoantigen clonality and quality[28].

We found a significant consolidation of neoantigen diversity among ICI-responsive CR tumors mirrored by a diversification of neoantigens among non-CR tumors. Tumor burden in CR versus non-CR tumors may underlie this observation, as responding tumors that rapidly lose cells also lose opportunities to gain new neoantigens, suppress extant neoantigens, and suppress HLA alleles[29]. Interestingly, we also found most tumors to possess at least one highly immunogenic subclonal neoantigen. While these neoantigens might be “confirmed” as immunogenic in ex vivo assays, they would be unlikely to instigate deep antitumor responses in vivo due to their lower clonality[6]. This provides additional impetus for considering the clonality of neoantigen expression in addition to transcript abundance writ large[2, 8, 30]. Our results quantify others’ findings that pre-treatment neoantigen clonality and quality affect ICI outcomes and caution against overreliance on confirmation of immunogenicity via ex vivo assays that cannot capture neoantigen clonality.

The simplifications we use for modeling introduce several limitations to our study. Chiefly, we do not consider spatial variation in neoantigen expression, which can cause heterogenous anti-tumor immunity, nor do we consider driver mutations that might elevate birth rates. Differential net birth rates, however, are captured in our model through presentome-

specific death rates among lineages within a tumor. On neoantigen expression, recent murine studies indicate that poor expression of clonal neoantigens can stunt anti-tumor immunity, supporting the need to represent expression levels with more granularity (i.e., as a continuous variable)[30]. We also did not consider genome doubling events, which cause greater expression of neoantigens developed prior to doubling[28]. Future work with our model could incorporate these features to capture their attendant effects on tumor heterogeneity.

In summary, we have developed a tumor growth model that tracks neoantigen clonality and accommodates tumor-level immunodominance among neoantigens. Our reduced representation of the tumor presentome can be readily adapted to simulate the interactions of other therapeutic modalities that induce antigen-specific anti-tumor immunity (e.g., vaccine) and the heterogenous neoantigen architectures of metastatic lesions and cancer types[31]. A greater understanding of intra- and intertumoral neoantigen evolution under therapy may inform novel therapeutic strategies that elicit more deep and durable responses.

DECLARATIONS

Patient consent for publication

Not applicable.

Ethics approval

Not applicable.

Availability of data and material

All original code has been deposited at Zenodo (doi: 10.5281/zenodo.5786469) and is publicly available. All data collected for simulation benchmarking and desired additional information are available from the lead contact upon request.

Competing interests

T.Q. is a shareholder of Humanigen (public biotechnology company), a consultant for Symberix (private biotechnology company), and a contractor for Hatteras Venture Partners (private financial services firm). B.V. is a shareholder of and consultant for GeneCentric (private biotechnology company). Y.C. is a consultant for Janssen Research & Development (subsidiary of Johnson & Johnson, a public pharmaceutical company).

Funding

This work was supported by the National Institute of Health (R35 GM119661).

Authors' contributions

Conceptualization, T.Q. and Y.C.; Methodology, T.Q.; Software, T.Q.; Validation, T.Q.; Formal Analysis, T.Q.; Investigation, T.Q.; Resources, Y.C.; Data Curation, T.Q.; Writing –

Original Draft, T.Q.; Writing – Review & Editing – T.Q., Y.C., and B.V.; Visualization – T.Q.; Supervision – Y.C.; Project Administration – T.Q. and Y.C.; Funding Acquisition – Y.C.

Acknowledgements

The authors thank Amber Cipriani and J. Justin Milner for their helpful input during study design and manuscript preparation.

SUPPLEMENTAL MATERIAL

Supplemental Item 1: Figure 1 Supporting Data, related to Figure 1.

Supplemental Item 2: Figure 2 Supporting Data, related to Figure 2.

Supplemental Item 3: Figure 3 Supporting Data, related to Figure 3.

Supplemental Tables and Figures: Table S1.

MAIN FIGURES

Figure 1. Recapitulation of untreated NSCLC neoantigen architecture in silico

A. Illustrative schematic of simulated tumor growth and neoantigen architecture. A founder cell is established with a random number of neoantigens. Each neoantigen has features drawn from the distributions reported for NSCLC tumors in Wells et al. At each time increment, the tumor dominant antigen (TDA) is calculated from the neoantigens with the most significant clonal fraction (cellularity). Cells that do not present TDAs are not selected against during cell killing, regardless of their non-TDA neoantigen burden. See Methods for further details.

B. Distribution of five key peptide features of NSCLC identified by Wells et al. 2020 (gray, top row). Overlaid in cyan are the sample distributions (cyan, top row). The parameter values of sampled peptide features are ranked and plotted (bottom row).

C. Distribution of tumor stages in TRACERx 100 cohort of NSCLC. Tumors of a given stage were simulated based on target diameters of 1.5 cm (stage IA), 3.5 cm (stage IB), 4.5 cm (stage IIA), and 5 cm (stage IIB/III).

D. Total neoantigen diversity in 100 simulated tumors, divided into clonal (blue) and subclonal (red) neoantigens. The overlaid navy line represents the distribution of total neoantigen diversity in a 55-tumor subset of the TRACERx 100 cohort, previously reported by Rosenthal et al. 2019.

E. Fraction of simulated tumors with clonal (blue) and subclonal (red) loss of at least one HLA allele. The fraction of tumors within the TRACERx 100 cohort with clonal and subclonal HLA loss of heterozygosity, previously reported by McGranahan et al. 2017, is shown for comparison.

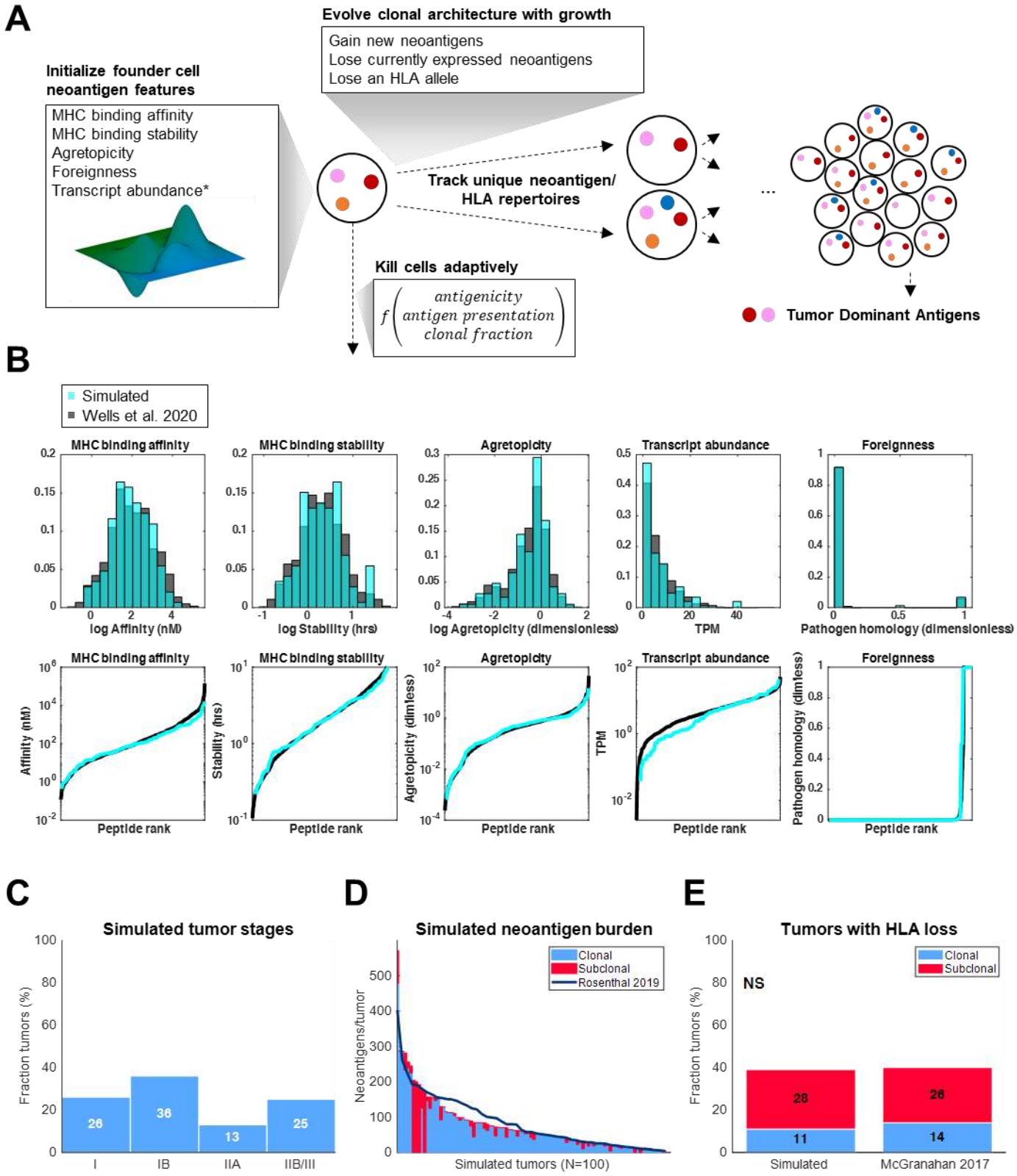
A
Evolve clonal architecture with growth
Gain new neoantigens
Lose currently expressed neoantigens
Lose an HLA allele
Initialize founder cell neoantigen features
MHC binding affinity
MHC binding stability
Agretopicity
Foreignness
Transcript abundance*
Track unique neoantigen/ HLA repertoires
Kill cells adaptively
$f\begin{pmatrix} antigenicity \\ antigen\ presentation \\ clonal\ fraction \end{pmatrix}$
Tumor Dominant Antigens
B
Simulated
Wells et al. 2020
MHC binding affinity
log Affinity (nM)
MHC binding stability
log Stability (hrs)
Agretopicity
log Agretopicity (dimensionless)
Transcript abundance
TPM
Foreignness
Pathogen homology (dimensionless)
Affinity (nM)
Stability (hrs)
Agretopicity (dimless)
Pathogen homology (dimless)
Peptide rank
C
Simulated tumor stages
Fraction tumors (%)
26
36
13
25
I
IB
IIA
IIB/III
D
Simulated neoantigen burden
Clonal
Subclonal
Rosenthal 2019
Neoantigens/tumor
Simulated tumors (N=100)
E
Tumors with HLA loss
Clonal
Subclonal
NS
Fraction tumors (%)
28
11
26
14
Simulated
McGranahan 2017

1

2

Figure 2. Validation of simulated pretreatment neoantigen burdens in a second cohort

A. Illustrative schematic of simulated tumor growth and neoantigen architecture in validation cohort of NSCLCs. For each of 12 patients in Forde Et al. 2018 with sufficient pretreatment tissue to characterize candidate neoantigens, tumor sizes were estimated; a cohort of 100 tumors was simulated for each size. As biopsies were single-region, neoantigen clonality was not assessed.

B. Distribution of simulated total neoantigen burden in 100-tumor cohorts of increasing size. Dashed lines represent neoantigen counts derived from raw data reported by Forde et al. 2018.

C. Distribution of simulated presentome neoantigen burden in 100-tumor cohorts of increasing size. Dashed lines represent neoantigen counts derived from raw data reported by Forde et al. 2018 that passed three of five Wells criteria (MHC binding affinity < 34 nM, MHC binding stability > 1.4 hours, and agretopicity > 0.1). In the absence of reported foreignness (pathogen homology), a correction factor equal to ratio of neoantigens in the Rosenthal et al. 2019 cohort passing the MHC binding affinity, stability, and agretopicity criteria that also did or did not adhere to the foreignness threshold of $< 10^{-16}$ was applied, reducing the number of predicted presentome antigens by 80.6%. Note: two tumors of 4 cm diameter had 2 presentome neoantigens.

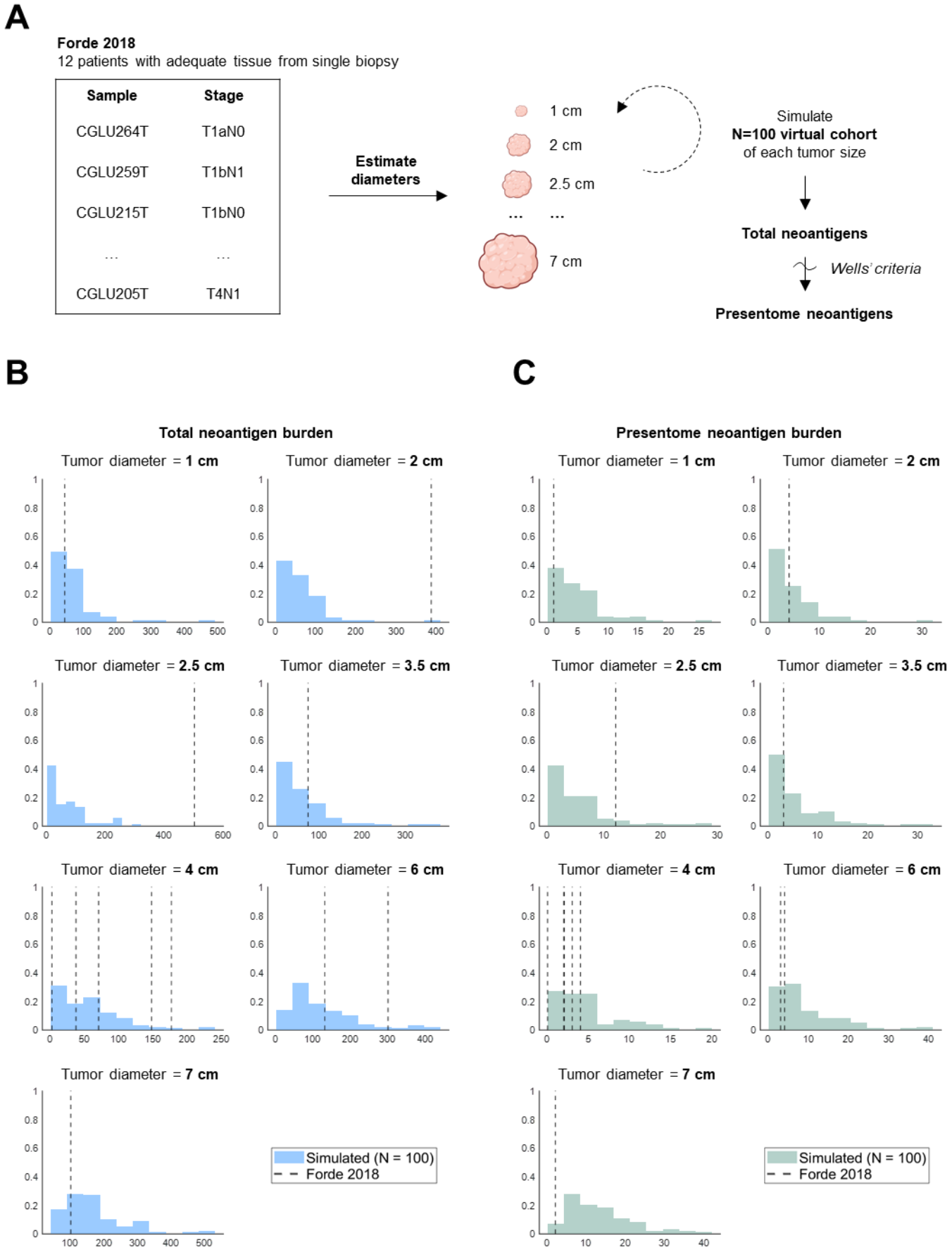
A
Forde 2018
12 patients with adequate tissue from single biopsy
Sample
Stage
CGLU264T
T1aN0
CGLU259T
T1bN1
CGLU215T
T1bN0
...
...
CGLU205T
T4N1
Estimate diameters
1 cm
2 cm
2.5 cm
...
...
7 cm
Simulate
N=100 virtual cohort
of each tumor size
Total neoantigens
Wells' criteria
Presentome neoantigens
B
Total neoantigen burden
Tumor diameter = 1 cm
Tumor diameter = 2 cm
Tumor diameter = 2.5 cm
Tumor diameter = 3.5 cm
Tumor diameter = 4 cm
Tumor diameter = 6 cm
Tumor diameter = 7 cm
Simulated (N = 100)
Forde 2018
C
Presentome neoantigen burden
Tumor diameter = 1 cm
Tumor diameter = 2 cm
Tumor diameter = 2.5 cm
Tumor diameter = 3.5 cm
Tumor diameter = 4 cm
Tumor diameter = 6 cm
Tumor diameter = 7 cm
Simulated (N = 100)
Forde 2018

1

Figure 3. Immune checkpoint inhibition simulations and correlates of response

A. Illustrative schematic of tumor treatment simulations. 1,051 advanced NSCLCs were simulated (diameter > 5 cm) and placed on virtual immune checkpoint inhibition (ICI) for 54 weeks. Clones harboring TDAs at the start of ICI were selected against for the duration of treatment. Every 9 weeks, tumor diameters were assessed and responses were classified per RECIST v1.1.

B. Simulated responses to ICI as determined by RECIST v1.1. “PD” includes tumors that experienced a diameter increase of at least 20% and 0.5 cm from simulation nadir. Simulated outcomes were statistically but not meaningfully different from outcomes reported in the literature, as determined by chi-square test.

C. Tumor growth trajectories of simulated tumors under treatment. For visualization, only 10% of 1051 simulated trajectories are shown.

D. Waterfall plot of responses to ICI. Colors indicate RECIST v1.1 classifications, with the threshold for CR estimated from an assumed diameter of 5 cm and detection limit of 0.2 cm.

E. Correlation of outcomes with pre-treatment TDA immunogenicity, as summarized by Pearson’s correlation coefficient. Immunogenicity units are arbitrary. Better outcomes correlated with greater more immunogenic pre-treatment TDAs.

F. Simulated responses to ICI as determined by RECIST v1.1 segmented by pre-treatment TDA expression. TDA loss fraction refers to the fraction of cells per simulated tumor that have lost expression of at least 1 TDA. “PD” includes tumors that experienced a diameter increase of at least 20% and 0.5 cm from simulation nadir. Simulated outcomes were statistically different between groups, as determined by chi-square test.

G. Simulated responses to ICI as determined by RECIST v1.1 segmented by pre-treatment HLA status. HLA loss fraction refers to the fraction of cells per simulated tumor that have expression of at least 1 HLA allele. “PD” includes tumors that experienced a diameter

increase of at least 20% and 0.5 cm from simulation nadir. Simulated outcomes were not statistically different between groups, as determined by chi-square test.

H. Correlation of outcomes with pre- and post-treatment total neoantigen, clonal neoantigen, subclonal neoantigen, and clonal reactive neoantigen burdens, as summarized by Pearson's correlation coefficient.

I. Select pre-treatment, post-treatment, and constant parameters of simulated complete responders (CR) versus all other simulated tumors (non-CR). Each cluster of bars is normalized to the pooled means of values across CR and non-CR tumors alike. This was further stratified by pre- and post-treatment status, with the exceptions of birth rate and NA gain rate, which were fixed during treatment. NA, neoantigen.

J. Significance of differences in evaluated parameters between pre- versus post-treatment tumors (top, paired t-test) and between CR versus non-CR tumors (bottom, unpaired t-test), as reported in panel E. Significance thresholds were Bonferroni corrected.

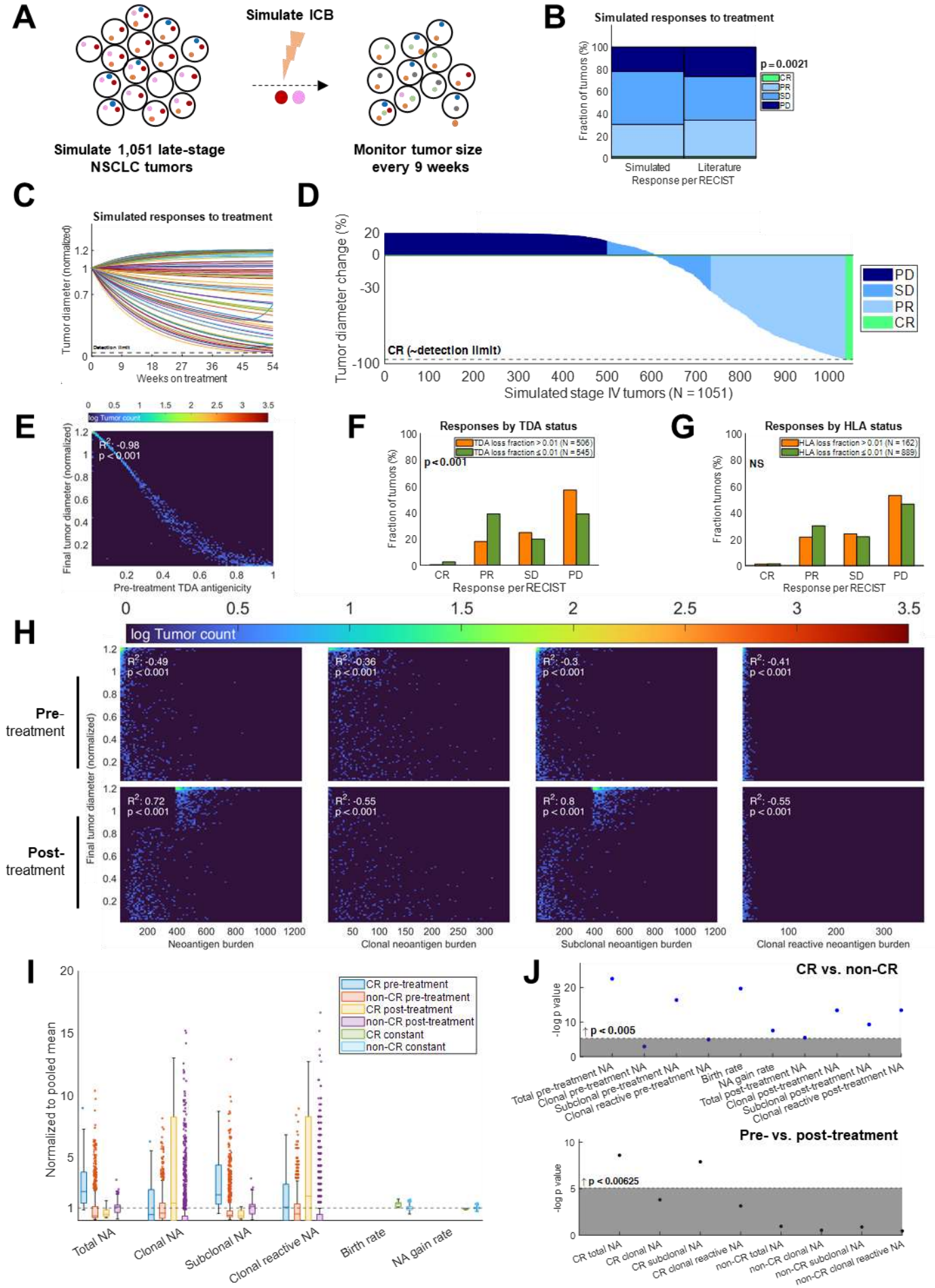
A
Simulate ICB
Simulate 1,051 late-stage NSCLC tumors
Monitor tumor size every 9 weeks
B
Simulated responses to treatment
Fraction of tumors (%)
p = 0.0021
CR
PR
SD
PD
Simulated
Literature
Response per RECIST
C
Simulated responses to treatment
Tumor diameter (normalized)
Weeks on treatment
D
Tumor diameter change (%)
CR (~detection limit)
Simulated stage IV tumors (N = 1051)
E
log Tumor count
R2: -0.98
p < 0.001
Final tumor diameter (normalized)
Pre-treatment TDA antigenicity
F
Responses by TDA status
TDA loss fraction > 0.01 (N = 506)
TDA loss fraction ≤ 0.01 (N = 545)
p < 0.001
Fraction of tumors (%)
Response per RECIST
G
Responses by HLA status
HLA loss fraction > 0.01 (N = 162)
HLA loss fraction ≤ 0.01 (N = 889)
NS
Fraction tumors (%)
Response per RECIST
H
log Tumor count
Pre-treatment
Post-treatment
Final tumor diameter (normalized)
R2: -0.49
p < 0.001
R2: -0.36
p < 0.001
R2: -0.3
p < 0.001
R2: -0.41
p < 0.001
R2: 0.72
p < 0.001
R2: -0.55
p < 0.001
R2: 0.8
p < 0.001
R2: -0.55
p < 0.001
Neoantigen burden
Clonal neoantigen burden
Subclonal neoantigen burden
Clonal reactive neoantigen burden
I
Normalized to pooled mean
CR pre-treatment
non-CR pre-treatment
CR post-treatment
non-CR post-treatment
CR constant
non-CR constant
Total NA
Clonal NA
Subclonal NA
Clonal reactive NA
Birth rate
NA gain rate
J
CR vs. non-CR
-log p value
p < 0.005
Total pre-treatment NA
Clonal pre-treatment NA
Subclonal pre-treatment NA
Clonal reactive pre-treatment NA
Birth rate
NA gain rate
Total post-treatment NA
Clonal post-treatment NA
Subclonal post-treatment NA
Clonal reactive post-treatment NA
Pre- vs. post-treatment
-log p value
p < 0.00625
CR total NA
CR clonal NA
CR subclonal NA
CR clonal reactive NA
non-CR total NA
non-CR clonal NA
non-CR subclonal NA
non-CR clonal reactive NA

Figure 4. Additional simulated outcomes and sensitivity analyses

A. Fraction of tumors before and after treatment with at least one subdominant TDA candidate. “Subdominant TDA candidate” refers to antigens in a tumor with greater immunogenicity but lower clonality than TDAs in the same tumor. Significance was assessed by chi-square test.

B. Sensitivity analysis of select model assumptions and parameters, including TDA oligoclonality, TDA number, birth rate, neoantigen gain rate, neoantigen loss rate, HLA loss rate, and treatment strength. When significant differences were present, individual group differences from baseline simulations were evaluated by post-hoc, Bonferroni-corrected chi-square test.

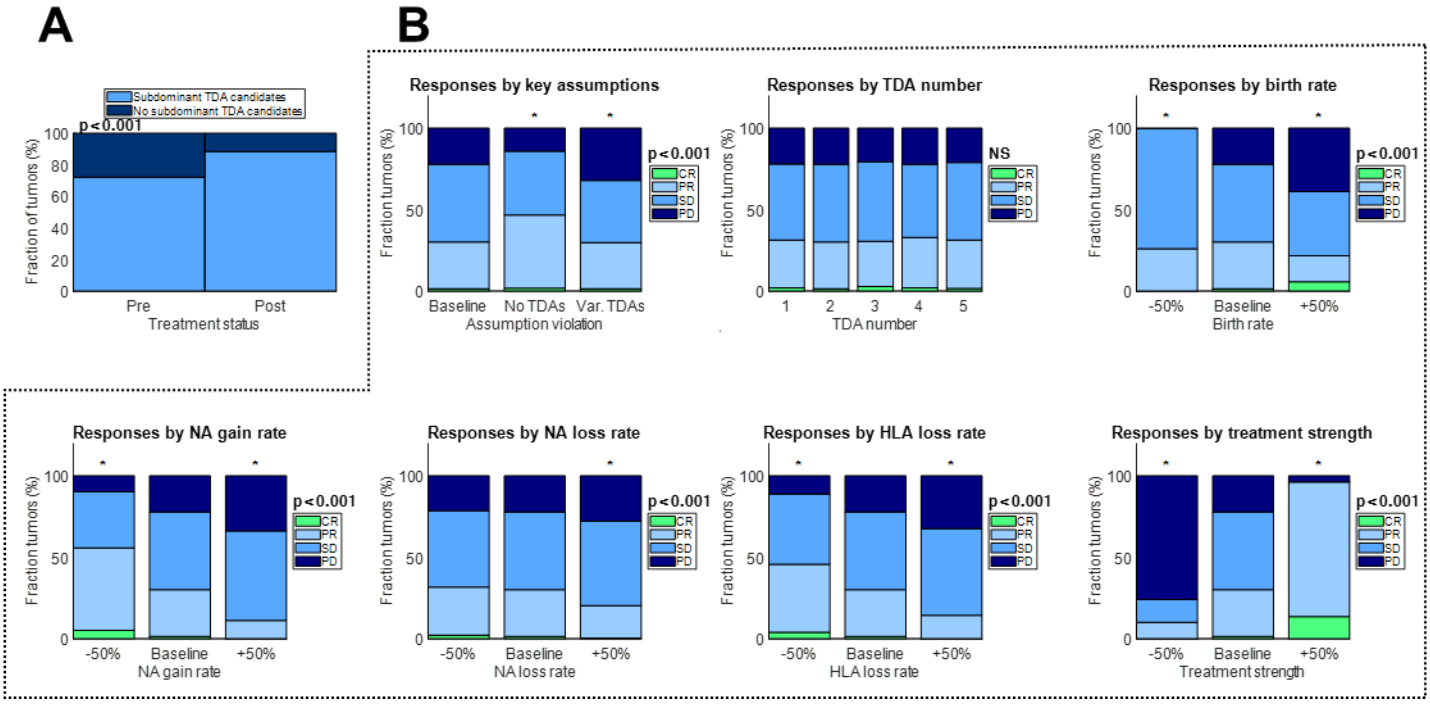
A
B
Subdominant TDA candidates
No subdominant TDA candidates
p<0.001
Fraction of tumors (%)
Pre
Post
Treatment status
Responses by key assumptions
Baseline
No TDAs
Var. TDAs
Assumption violation
Responses by TDA number
NS
TDA number
Responses by birth rate
-50%
+50%
Birth rate
Responses by NA gain rate
NA gain rate
Responses by NA loss rate
NA loss rate
Responses by HLA loss rate
HLA loss rate
Responses by treatment strength
Treatment strength
Fraction tumors (%)
CR
PR
SD
PD

SUPPLEMENTAL TABLES AND FIGURES

Table S1. Simulated tumor parameters, related to Methods

Parameters	Value (units)	Source	Notes
Birth rate, deathless	0.4 (1/day)	Avanzini and Antal 2019	Lognormally distributed
Birth rate log standard deviation	0.2	Manually estimated	
Death rate	0.36 (1/day)	Avanzini and Antal 2019	Always 90% of sampled deathless birth rate
Cell volume	4.19 (pL)	Molecular Cell Biology, 4th Ed.	Assumes spherical tumor
Carrying capacity	10^{12} (cells)	Zinner et al. 2015 available from doi.org/10.34949/fv7a-0v28	Estimated from diameters of 10 largest tumors
Neoantigen gain rate	5×10^{-11} (1/day)	Manually estimated	
Neoantigen gain rate log standard deviation	0.1	Manually estimated	
Founding neoantigen number shape parameter	1.14	Fit to Rosenthal et al. 2019	Parameterizes gamma distribution
Founding neoantigen number scale parameter	56.24	Fit to Rosenthal et al. 2019	Parameterizes gamma distribution
Neoantigen loss rate	3.35×10^{-11} (1/day)	Fit to Rosenthal et al. 2019	Always 67% of sampled neoantigen gain rate, as 33% of genomically clonal neoantigens were found to be transcriptomically clonal
HLA loss rate	3.35×10^{-11} (1/day)	Fit to McGranahan et al. 2017	Same as neoantigen loss rate
TDA number	2	Estimated from McGranahan et al. 2016; Lo et al. 2021	
Treatment strength	8 (%)	Manually estimated	Linear amplification of death rate

REFERENCES

[1] J. H. Strickler, B. A. Hanks, and M. Khasraw, “Tumor Mutational Burden as a Predictor of Immunotherapy Response: Is More Always Better?,” *Clin. Cancer Res.*, vol. 27, no. 5, pp. 1236–1241, Mar. 2021, doi: 10.1158/1078-0432.CCR-20-3054.

[2] N. McGranahan *et al.*, “Clonal neoantigens elicit T cell immunoreactivity and sensitivity to immune checkpoint blockade,” *Science*, vol. 351, no. 6280, pp. 1463–1469, 2016.

[3] C. C. Smith, S. R. Selitsky, S. Chai, P. M. Armistead, B. G. Vincent, and J. S. Serody, “Alternative tumour-specific antigens,” *Nat. Rev. Cancer*, vol. 19, no. 8, pp. 465–478, Aug. 2019, doi: 10.1038/s41568-019-0162-4.

[4] V. Anagnostou *et al.*, “Evolution of Neoantigen Landscape during Immune Checkpoint Blockade in Non–Small Cell Lung Cancer,” *Cancer Discov.*, vol. 7, no. 3, pp. 264–276, Mar. 2017, doi: 10.1158/2159-8290.CD-16-0828.

[5] K. Litchfield *et al.*, “Meta-analysis of tumor- and T cell-intrinsic mechanisms of sensitization to checkpoint inhibition,” *Cell*, vol. 184, no. 3, pp. 596-614.e14, Feb. 2021, doi: 10.1016/j.cell.2021.01.002.

[6] R. S. Gejman *et al.*, “Rejection of immunogenic tumor clones is limited by clonal fraction,” *eLife*, vol. 7, p. e41090, Nov. 2018, doi: 10.7554/eLife.41090.

[7] C. C. Smith *et al.*, “Machine-Learning Prediction of Tumor Antigen Immunogenicity in the Selection of Therapeutic Epitopes,” *Cancer Immunol. Res.*, vol. 7, no. 10, pp. 1591–1604, Oct. 2019, doi: 10.1158/2326-6066.CIR-19-0155.

[8] D. K. Wells *et al.*, “Key Parameters of Tumor Epitope Immunogenicity Revealed Through a Consortium Approach Improve Neoantigen Prediction,” *Cell*, vol. 183, no. 3, pp. 818-834.e13, Oct. 2020, doi: 10.1016/j.cell.2020.09.015.

[9] H. Schreiber, T. H. Wu, J. Nachman, and W. M. Kast, “Immunodominance and tumor escape,” *Semin. Cancer Biol.*, vol. 12, no. 1, pp. 25–31, Feb. 2002, doi: 10.1006/scbi.2001.0401.

[10] J. Friedman *et al.*, “Neoadjuvant PD-1 Immune Checkpoint Blockade Reverses Functional Immunodominance among Tumor Antigen–Specific T Cells,” *Clin. Cancer Res.*, vol. 26, no. 3, pp. 679–689, Feb. 2020, doi: 10.1158/1078-0432.CCR-19-2209.

[11] N. McGranahan *et al.*, “Allele-Specific HLA Loss and Immune Escape in Lung Cancer Evolution,” *Cell*, vol. 171, no. 6, pp. 1259-1271.e11, Nov. 2017, doi: 10.1016/j.cell.2017.10.001.

[12] R. Rosenthal *et al.*, “Neoantigen-directed immune escape in lung cancer evolution,” *Nature*, vol. 567, no. 7749, pp. 479–485, Mar. 2019, doi: 10.1038/s41586-019-1032-7.

[13] P. M. Forde *et al.*, “Neoadjuvant PD-1 Blockade in Resectable Lung Cancer,” *N. Engl. J. Med.*, vol. 378, no. 21, pp. 1976–1986, May 2018, doi: 10.1056/NEJMoa1716078.

[14] S. Avanzini and T. Antal, “Cancer recurrence times from a branching process model,” *PLOS Comput. Biol.*, vol. 15, no. 11, p. e1007423, Nov. 2019, doi: 10.1371/journal.pcbi.1007423.

[15] H. F. Lodish, Ed., *Molecular cell biology*, 4th ed. New York: W.H. Freeman, 2000.

[16] M. Rasmussen *et al.*, “Pan-Specific Prediction of Peptide–MHC Class I Complex Stability, a Correlate of T Cell Immunogenicity,” *J. Immunol.*, vol. 197, no. 4, pp. 1517–1524, Aug. 2016, doi: 10.4049/jimmunol.1600582.

[17] M. B. Amin, American Joint Committee on Cancer, and American Cancer Society, Eds., *AJCC cancer staging manual*, Eight edition / editor-In-Chief, Mahul B. Amin, MD, FCAP ; Editors, Stephen B. Edge, MD, FACS [and 16 others] ; Donna M. Gress, RHIT, CTR-Technical editor ; Laura R. Meyer, CAPM-Managing editor. Chicago IL: American Joint Committee on Cancer, Springer, 2017.

[18] D. P. Carbone *et al.*, “First-Line Nivolumab in Stage IV or Recurrent Non–Small-Cell Lung Cancer,” *N. Engl. J. Med.*, vol. 376, no. 25, pp. 2415–2426, Jun. 2017, doi: 10.1056/NEJMoa1613493.

[19] T. S. K. Mok *et al.*, “Pembrolizumab versus chemotherapy for previously untreated, PD-L1-expressing, locally advanced or metastatic non-small-cell lung cancer (KEYNOTE-042): a randomised, open-label, controlled, phase 3 trial,” *The Lancet*, vol. 393, no. 10183, pp. 1819–1830, May 2019, doi: 10.1016/S0140-6736(18)32409-7.

[20] M. Reck *et al.*, “Five-Year Outcomes With Pembrolizumab Versus Chemotherapy for Metastatic Non–Small-Cell Lung Cancer With PD-L1 Tumor Proportion Score ≥ 50%,” *J. Clin. Oncol.*, vol. 39, no. 21, pp. 2339–2349, Jul. 2021, doi: 10.1200/JCO.21.00174.

[21] N. A. Rizvi *et al.*, “Durvalumab With or Without Tremelimumab vs Standard Chemotherapy in First-line Treatment of Metastatic Non–Small Cell Lung Cancer: The MYSTIC Phase 3 Randomized Clinical Trial,” *JAMA Oncol.*, vol. 6, no. 5, p. 661, May 2020, doi: 10.1001/jamaoncol.2020.0237.

[22] A. A. Lo *et al.*, “Indication-specific tumor evolution and its impact on neoantigen targeting and biomarkers for individualized cancer immunotherapies,” *J. Immunother. Cancer*, vol. 9, no. 10, p. e003001, Oct. 2021, doi: 10.1136/jitc-2021-003001.

[23] M. Jamal-Hanjani *et al.*, “Tracking the Evolution of Non-Small-Cell Lung Cancer,” *N. Engl. J. Med.*, vol. 376, no. 22, pp. 2109–2121, Jun. 2017, doi: 10.1056/NEJMoa1616288.

[24] E. A. Eisenhauer *et al.*, “New response evaluation criteria in solid tumours: revised RECIST guideline (version 1.1),” *Eur. J. Cancer Oxf. Engl. 1990*, vol. 45, no. 2, pp. 228–247, Jan. 2009, doi: 10.1016/j.ejca.2008.10.026.

[25] G. Aguadé-Gorgorió and R. Solé, “Tumour neoantigen heterogeneity thresholds provide a time window for combination immunotherapy,” *J. R. Soc. Interface*, vol. 17, no. 171, p. 20200736, Oct. 2020, doi: 10.1098/rsif.2020.0736.

[26] E. Lakatos *et al.*, “Evolutionary dynamics of neoantigens in growing tumors,” *Nat. Genet.*, vol. 52, no. 10, pp. 1057–1066, Oct. 2020, doi: 10.1038/s41588-020-0687-1.

[27] M. Łuksza *et al.*, “A neoantigen fitness model predicts tumour response to checkpoint blockade immunotherapy,” *Nature*, vol. 551, no. 7681, pp. 517–520, Nov. 2017, doi: 10.1038/nature24473.

[28] N. McGranahan and C. Swanton, “Neoantigen quality, not quantity,” *Sci. Transl. Med.*, vol. 11, no. 506, p. eaax7918, Aug. 2019, doi: 10.1126/scitranslmed.aax7918.

[29] F. G. Dall’Olio *et al.*, “Tumour burden and efficacy of immune-checkpoint inhibitors,” *Nat. Rev. Clin. Oncol.*, Oct. 2021, doi: 10.1038/s41571-021-00564-3.

[30] P. M. K. Westcott *et al.*, “Low neoantigen expression and poor T-cell priming underlie early immune escape in colorectal cancer,” *Nat. Cancer*, vol. 2, no. 10, pp. 1071–1085, Oct. 2021, doi: 10.1038/s43018-021-00247-z.

[31] Z. Hu, Z. Li, Z. Ma, and C. Curtis, “Multi-cancer analysis of clonality and the timing of systemic spread in paired primary tumors and metastases,” *Nat. Genet.*, vol. 52, no. 7, pp. 701–708, Jul. 2020, doi: 10.1038/s41588-020-0628-z.

[32] R. G. Zinner *et al.*, “PRONOUNCE: randomized, open-label, phase III study of first-line pemetrexed + carboplatin followed by maintenance pemetrexed versus paclitaxel + carboplatin + bevacizumab followed by maintenance bevacizumab in patients ith advanced nonsquamous non-small-cell lung cancer,” *J. Thorac. Oncol. Off. Publ. Int. Assoc. Study Lung Cancer*, vol. 10, no. 1, pp. 134–142, Jan. 2015, doi: 10.1097/JTO.0000000000000366.